doi.org/10.36721/PJPS.2026.39.7.183.1

Nano-scaffolds for enhanced *in-vitro* and *in-vivo* anti-VEGFR drug delivery

Arooj Khalid[1], Muhammad Yasir Ali[1*], Romna tul Janat[1], Mulazim Hussain Asim[2], Ijaz Ali[1], Daulat Haleem Khan[3], Umaira Rehman[3], Saima[3] and Asma Razzaq[3]

[1]Faculty of Pharmaceutical Sciences, GC University Faisalabad, Faisalabad, Punjab, Pakistan
[2]College of Pharmacy, University of Sargodha, Sargodha, Punjab, Pakistan
[3]Lahore College for Pharmaceutical Sciences, Lahore, Punjab, Pakistan

Abstract: **Background**: Sorafenib (SB) is a receptor tyrosine kinase inhibitor, currently marketed as an oral dosage form. However, due to severe irritation of the gastrointestinal tract, the drug is facing decreased acceptability as a therapeutic agent. **Objectives**: This study aimed to develop nano-scaffolds to increase the drug loading capacity and decrease the adverse drug reactions of SB. **Method**: Polymers used for the preparation of nano-scaffolds were polylactic co-glycolic acid (PLGA), ethyl cellulose (EC) and polyvinyl alcohol which was used as a surfactant. A range of different formulations was designed using 12.5 mg and 25 mg of EC, while the concentration of the PLGA was kept constant throughout the study. All formulations with or without the drug were characterized for size by dynamic light scattering (DLS), scanning electron microscopy, differential scanning calorimetry, hemolysis assay, cell viability assay, apoptotic assay and *in-vivo* evaluation. **Results**: DLS results showed the minimum nano-scaffold size of 252.8 ± 12 nm, which was increased by increasing the concentration of polymer and drug. The physicochemical assessment showed the presence of minor interactions between the polymeric system and SB. The cell viability assay showed the minimum cell viability at 50.66 ± 0.13 % at a maximum concentration of SB-loaded formulations, whereas the presence of apoptotic bodies confirmed these results. **Conclusion**: The *in-vitro* and *in-vivo* evaluation showed the safety profile of the polymeric PLGA/EC in the absence of drug content. Therefore, the fabricated system may be used as a carrier system for SB and can further be included in tumor model studies.

Keywords: Apotptosis; Clinical markers; Cell viability; *Ex-vivo* hemolysis

Submitted on 23-09-2025 – Revised on 30-01-2026 – Accepted on 06-02-2026

INTRODUCTION

Chemotherapeutic substances have no site-specific reaction that results in increasing the emergence of a targeted drug delivery system to decrease tissue toxicity. The formation of nanoparticles and liposomes has diverted the face of chemotherapy (Tupe *et al*., 2024). Different therapeutic agents are loaded into nanoparticles by the process of encapsulation or entrapment. Recent advancements in cancer therapy are the preparation of various types of nano-scaffolds for anti-tumor activity, such as polymeric nano-scaffolds, fibrous nano-scaffolds, hydrogel nano-scaffolds and microsphere scaffolds. PLGA, polyglycolic acid and polylactic acid (PLA) are widely used polymers for the formulation of nanoparticles because of their biodegradability and biocompatibility. Among all these, the most commonly used material is PLGA, which is required for the formation of nanoparticles and nano-scaffolds. A major challenge that can be confronted is the development of nano-scaffolds with a tumor-specific ligand (Li *et al*., 2025).

A nano-scaffold is a three-dimensional structure having a pore size of 1-1000 nm and it serves as a carrier for a drug to the site of action. The porous structure of the nano-scaffold significantly influences cell migration, proliferation and vascularization (Dwivedi *et al*., 2020). It should have homogeneous drug dispersion throughout the structure, a high porosity level, physical and chemical stability and biological stability over an extended period, and a high capacity to release the drug at a therapeutic level. A major purpose for the formation of nano-scaffolds is to target and increase the uptake of antitumor agents, prolong the drug effect, target intracellular infections, enhance immune response, increase bioavailability, reduce the washout period and improve drug retention and absorption (Donnaloja *et al*., 2020).

The main aim of the current study was to develop nano-scaffolds to increase the drug loading capacity and decrease the adverse drug reactions of SB. Polymers used during the current study were PLGA, EC and polyvinyl alcohol (PVA). EC is used to prepare a matrix and nano-scaffolds. It is also used in the coating of different nanoparticles for targeted effects (Tong *et al*., 2025). SB is a multi-kinase inhibitor that blocks VEGFR. Due to the inhibition of the VEGFR receptor, the process of angiogenesis and cell proliferation is blocked. The major drawback of SB therapy is resistance due to having no drug specificity to the drug delivery site. Hence, SB-loaded nano-scaffolds can be formed to overcome this resistance and adverse drug reactions (Zengin Kurt *et al*., 2024). In the current study, the nano-scale scaffolds were prepared by the solvent evaporation method and then were further characterized using physicochemical techniques. These

**Corresponding author:* e-mail: m.yasirali14@gmail.com

evaluation parameters were dynamic light scattering, scanning electron microscopy and DSC. Furthermore, the evaluation was carried out by *in-vitro* cell culture studies and *in-vivo* mouse models (Guzman-Rocha *et al*., 2025; Mohaghegh *et al*., 2024).

MATERIALS AND METHODS

Materials

EC (48.0-49.5%), PLGA (R503H, Mw30 kDa), 3-(4,5-dimethyl-2-thiazolyl)-2,5-diphenyl-2H-tetrazolium bromide (MTT), 4′,6-diamidino-2-phenylindole (DAPI), tert-butyl hydroperoxide (TBHP), sodium chloride, potassium chloride, potassium dihydrogen phosphate, PVA (Mowiol 4-88) and Triton X-100 were purchased from Sigma Aldrich (Darmstadt, Germany). SB was purchased from LC Laboratories (Woburn, USA). Ethyl acetate was obtained from Chemsolute-Th. Geyer (Renningen, Germany), while tetrahydrofuran and ethanol were purchased from Carl Roth (Karlsruhe, Germany) and Thermo Fisher (Waltham, UK). DMEM cell culture medium was obtained from Capricorn Scientific (Ebsdorfergrund, Germany). All the reagents used were of analytical grade.

Cell lines and cell culture

The human HepG2 liver cancer cells (ATCC, Manassas, USA) were cultured in Dulbecco's Modified Eagle's Medium (DMEM) supplemented with 10 % fetal bovine serum (FBS), 100 units/mL penicillin and 100 ug/mL streptomycin and maintained at 37°C ± 0.5 having 5 % CO_2 in a humidified atmosphere (Gordon and Amini, 2021). Supplier and short tandem repeat (STR) details are included in supplementary data.

Preparation of nano-scaffolds

Preparation of PLGA/EC nano-scaffolds was done by the solvent-evaporation method (Sathish *et al*., 2022). 500 µl of 1 % PVA stock solution was added to 4.5 ml of distilled water to make the final volume up to 5 ml of aqueous phase. 25 mg PLGA and 12.5 mg to 25 mg EC (2^3 factorial design, Table 1) were added to 5 ml ethyl acetate containing 5 mg of sodium chloride and mixed by magnetic stirring; in this way, an organic phase was obtained. This organic phase was added drop-wise to 5 ml of PVA aqueous solution, keeping the aqueous phase on a magnetic stirrer. The resultant emulsion was homogenized by an overhead homogenizer (Heidolph Instruments, Germany) at 9,000 rpm for 10 mins. After homogenization, 20 ml distilled water was added to facilitate the evaporation of the organic phase and left for overnight stirring with the magnetic stirrer. The complete evaporation of the organic phase resulted in the formation of nano-scaffolds. The drug-loaded nano-scaffolds were prepared by the same method except for the incorporation of drug solution in a tetrahydrofuran/ethanol co-solvent system in the organic phase. The rest of the method of preparation was the same. The prepared nano-scaffolds were washed with distilled water thrice and stored at 4°C until further use.

Table 1: Factorial design for formulation.

Formulations	SB	PVA	EC	SB (mg)	PVA (mg)	EC (mg)
F1	-	-	-	0	1.5	12.5
F2	+	-	-	1	1.5	12.5
F3	-	+	-	0	2	12.5
F4	+	+	-	1	2	12.5
F5	-	-	+	0	1.5	25
F6	+	-	+	1	1.5	25
F7	-	+	+	0	2	25
F8	+	+	+	1	2	25

Encapsulation efficiency

Briefly, washed nano-scaffolds were centrifuged at 14,000 rpm for 20 mins and the pellet was dissolved in tetrahydrofuran/ethanol. The samples were analyzed by a UV spectrophotometer (Shimadzu, Japan) at 256 nm and the concentration of the drug in a sample was calculated against the calibration curve of known concentrations of the drug. The encapsulation efficiency was evaluated by utilizing the following formula, performed in triplicate and the results were reported as mean and standard deviation (Ali *et al*., 2020).

$$\text{EE (\%)} = \frac{Amount\ of\ the\ drug\ present\ in\ scaffolds}{Amount\ of\ the\ drug\ added} \times 100$$

Determination of particle size

Dynamic light scattering (DLS) was used for the assessment of the size and size distribution of all formulations (Nano ZS, Malvern Instruments, Malvern, UK). All the samples were diluted with purified distilled water at a ratio of 1:100 and were analyzed. Before taking measurements, the sample temperature was adjusted to 25 °C and then all measurements were taken 3 times independently and the sub-runs were automatically adjusted by the instrument. By intensity distribution, size distribution was assessed in triplicate and reported (Ali *et al*., 2021).

Scanning electron microscopy (SEM)

SEM is one of the high-resolution electron microscopy techniques that helps to provide accurate information about nanoparticles by using a high-energy electron beam to probe samples on a very fine scale. Surface morphology, pore size and cellular attachment can be determined by using SEM. Under liquid nitrogen, the formulations were placed on aluminum stubs, air-dried and sputter-coated with gold under an atmosphere of argon by using high vacuum pressure. Then the samples were observed by a high-energy electron beam in SEM (Cube series, Emcrafts, South Korea) at 8-10 kV voltage and 15.92 to 16.20 mm working distance (Jamil *et al*., 2026).

Differential scanning calorimetry (DSC)

The nature of the excipients is inert; however, sometimes drug interaction with excipients can happen. Therefore, incompatibility between the drug and excipients can affect the physicochemical and other properties of the

formulation. Therefore, the compatibility between the drug and excipients and their effect on the stability of formulations can be determined by DSC (Microcal, Northampton, MA, USA). The scanning temperature range was between 0 and 250ºC with a heating rate of 1ºC per minute (Alawak *et al*., 2020). The reference cell was filled with equivalent distilled water and the baseline was measured to decrease the chance of error in samples.

Cell viability assay

Cell viability was evaluated by MTT assay using a HepG2 cell line. 1×10^4 cells/wells were seeded in 96-well plates and were incubated for 48 hrs at 37±0.5ºC. After 48 hrs of seeding, cells were washed three times with phosphate buffer (PBS, pH 7.4) and fresh DMEM-containing formulations (140 µg) were replenished. The treatment medium was removed after a 48 hrs incubation period, all the wells were washed with PBS, and 200 µL of 1 mg/ml MTT reagent in PBS (pH 7.4) was added to the wells. The medium was removed after the incubation for 3 hrs and 100 µL DMSO was added to solubilize the formazan crystals formed by live cells (Benov, 2021). All the plates were homogenized for 10 mins and the absorbance of each well was recorded in a plate reader at λ=570 nm (Ali *et al*., 2020). The assay was performed in triplicate and results were reported as mean and standard deviation.

Apoptotic assay

HepG2 cells were cultivated under a laminar flow hood on sterile and preheated coverslips in 12-well plates for 36 hrs with a cellular density of 12×10^4 cells per well. After the required confluency was attached, the cells were washed with ice-cold PBS (pH 7.4) thrice (Chen *et al*., 2022). Then, 200 µl of different formulations was added to different wells. After the incubation for 12 hrs, cells were washed again with ice-cold PBS (pH 7.4), fixed with 0.5 ml 4% paraformaldehyde for 15 mins and incubated with 300 µl DAPI (0.1 mg/ml) solution for 20 mins in the dark at 37 ± 0.5 °C. Washing was done with PBS (pH 7.4) and cells were examined using a fluorescent microscope (Olympus, USA).

Ex-vivo hemolysis assay

To evaluate the hemolytic potential of the nano-scaffolds on blood, erythrocytes were isolated from fresh human blood. An anonymous healthy male, age 30, was used to collect the fresh blood. (Wu *et al*., 2021). In EDTA tubes, fresh blood was taken to prevent coagulation and centrifuged to get plasma from the blood. The red blood cell pellet was obtained and washed three times with a phosphate buffer solution. For the sample analysis, 180 µL of RBCs pellet was mixed with a 20 µL formulation. The samples were centrifuged thrice for washing with PBS (pH 7.4) and the absorbance of the collected supernatant was determined at 540 nm. NaCl 0.9 % solution, untreated erythrocytes and 1 % Triton™ X-100 were utilized as controls and the values of absorbance of Triton™ X-100 were assumed as 100 % hemolysis. The assay was performed in triplicate and results were reported as mean and standard deviation.

Acute toxicity assessment

Female BALB/c mice of weight between 25-35 gm and age between 8-10 weeks were obtained from the animal laboratory of GC University, Faisalabad, Pakistan, after approval from the ethical committee of the university (00140/22/April 22). All the animals were divided into three different groups: the control group, the drug-loaded formulation-treated group and the drug-free formulation-treated group. Each group contained 3 mice and was kept with free access to water and food at a temperature of 22 ± 2ºC and with 12 hrs light and dark cycle (Malik *et al*., 2022). An equivalent dose of 25 mg/kg of SB was injected through the tail vein on day 1 (D1) and day 3 (D3). On day 7 (D7), all the animals were euthanized by cervical dislocation under Annex IV of Directive 2010/63/EU of the European Parliament and of the Council of 22 September 2010 on the protection of animals used for scientific purposes. The vital organs like lungs, heart, liver and kidneys were separated and the body viscera were calculated as follows;

$$\text{Body Viscera (\%)} = \frac{\text{Vital Organ Weight (gm)}}{\text{Total Body Weight (gm)}} \times 100$$

Clinical markers

Blood was collected from the mice by cardiac puncture and plasma was separated by centrifugation at 1000 g for 10 mins. Complete blood count, renal function test and liver function test were performed to evaluate the effect of formulations on these clinical markers (Ali *et al*., 2021).

Histopathological evaluation

After euthanizing the animals on day 7, the lungs, heart, liver and kidneys were removed and observed for any change in the histopathology of the organs. Briefly, organs were washed with PBS (pH 7.4) and stored in 4 % formalin for one day. After dehydration with ethanol, fixation was done in paraffin blocks. Thin sections were cut with a microtome and slides were prepared. H and E staining was performed and signs of toxicities were observed under a microscope (NOIF, XSZ-107BN, Zenith Lab Inc., China).

Statistical analysis

OriginLab8 was used for plotting the graphs and for statistical investigation. All the experiments were performed in triplicate and results were shown in the form of mean ± standard deviation, unless stated. One-way ANOVA was used to evaluate the statistical significance of the results. Statistical significance was represented in the form of probability value and shown as "*" $p < 0.05$, "**" $p < 0.01$ and "***" $p < 0.001$.

RESULTS

Preparation of nano-scaffolds

In cellular uptake of nano-scaffolds, size plays a vital role; hence, in preliminary experiments, the concentration of EC

and PVA utilized for the preparation of nano-scaffolds was adjusted. All the formulations were analyzed for size distribution (in preliminary experiments) by factorial design and it was found that by using drug solution THF: EtOH (20:5) with the organic phase of ethyl acetate, the lowest particle size was demonstrated (Anindyajati *et al*., 2022). The process of homogenization can further reduce the particle size of nano-scaffolds. Moreover, continuous stirring with homogenization and the addition of water increases the evaporation of the organic phase (Zhu *et al*., 2021). The resultant nano-scaffolds were then washed and utilized for further characterization both *in-vitro* and *in-vivo*.

Encapsulation efficiency (EE)

As encapsulation efficiency is the major challenging issue in the preparation of nano-scaffolds and nanoparticles because of the hydrophilic and lipophilic balance of any drug, EE was checked to get insight information on the drug loading. So, encapsulation of SB was 74.12 ± 2.59 % because SB has less solubility in water and more solubility in organic solvents; a high amount of the drug was encapsulated in the nano-scaffold (Baltz and Scherließ, 2025).

Determination of particle size

For the preparation of nano-scaffolds, the solvent evaporation method was used. To optimize the effect of PVA, drug content and concentration of EC, a 2^3 factorial design was used (F1 to F8), keeping PLGA concentration constant. It was obvious from this factorial design that by changing the concentration of EC, a more pronounced effect on the size and the PDI was present. This correlates with the water disintegration and erodability of EC in the aqueous phase (Lu, Zhang *et al*., 2023). After optimization, all formulations were evaluated for particle size, which was 252.8 ± 12 nm for blank formulation (F1). On the other hand, the size of the final selected formulation with drug (F6) was 500.8 ± 10 nm (Fig. 1A). These formulations were selected for all other experiments due to their good size and size distribution. PDI for these formulations was 0.09 ± 0.02 to 0.41 ± 0.10 for F1 and F6, respectively (Table S1).

Scanning electron microscopy

By using SEM, morphological characterization was performed. In this, 40 µl of concentrated samples were placed on carbon tabs and dried properly under a laminar airflow hood to maintain the structure and size of the nano-scaffolds. SEM micrograph showed the presence of single as well as fused particles; however, it was obvious that the particles present as single identity were round in shape (Fig. 1B). These images also represented the presence of porous surfaces of nano-scaffolds. The diameter was more than that of the diameter from the dynamic light scattering results. This might be due to the soft nature of particles that settled down on the surface of the aluminum stubs to increase their size.

Differential scanning calorimetry

To evaluate the elementary characterization of formulations like melting point, crystallization, fusion, etc, DSC is used (Yu *et al*., 2023). The DSC thermogram of SB elucidates that it has a sharp endothermic peak at 240.03℃, which exhibits the semicrystalline or amorphous nature of the SB. Moreover, in PLGA, there was a peak exhibiting a rigid chain structure having a glass transition temperature at 48.66 ℃; however, in the case of EC, there was a change in physical state at 193.73 ℃. The formulation containing the drug showed an endothermic peak of 116.2 ℃, representing the presence of an amorphous structure gaining crystallinity again (Fig. 2). Moreover, this peak was different from the peaks of the pure drug as well. These results showed the presence of some interaction between SB and excipients in the formulation under investigation. Moreover, the peak of the formulation showed a sharp endset gain, representing a small initial crystalline structure. All these results indicated a mixture of amorphous and crystal structures; therefore, a few molecules of the drug were interacting with the polymeric system and a few others were present as a physical mixture. This may predict the reason for the low EE% of SB despite its high lipophilicity.

Cell viability

To determine cell viability, an MTT assay was utilized to check the percentage of living cells at different concentrations (Kus-Liśkiewicz *et al*., 2021). A dose-response cell viability was observed by increasing the concentration of nano-scaffolds from 2.1875 µg to 140 µg (Fig. 3A). The results were statistically significant ($p < 0.001$) for both with and without drug formulations. However, the cell viability in the case of blank formulation was greater than 80 % in every treatment concentration. The maximum cell viability for F1 and F6 was 99.23 ± 0.37 % and 99.05 ± 0.78 %, respectively. On the other hand, the minimum cell viability of F1 and F6 at concentrations of 140 µg was 80.91 ± 2.41 % ($p < 0.001$) and 50.66 ± 0.13 % ($p < 0.001$), respectively. The cell viability in the case of equimolar concentration of SB was also observed for comparison and plotted in the same graph (Fig. 3A).

Apoptotic assay

The DAPI staining was used for the assessment of the mechanism of killing the cells. The nucleus of the cells can be stained with DAPI and thus can be visualized by a microscope for the assessment of nuclear condensation (decrease in nuclear size) and chromatin degradation (formation of different fragmentation). These results represent the formation of apoptotic bodies and the ultimate mechanism of cell death (Estandarte *et al*., 2016; Huang *et al*., 2014). It was observed during DAPI staining that a reasonable amount of the apoptotic bodies were formed, after treatment with F6 (Fig. 3B). DAPI stains the degraded chromatin materials more than normal cells.

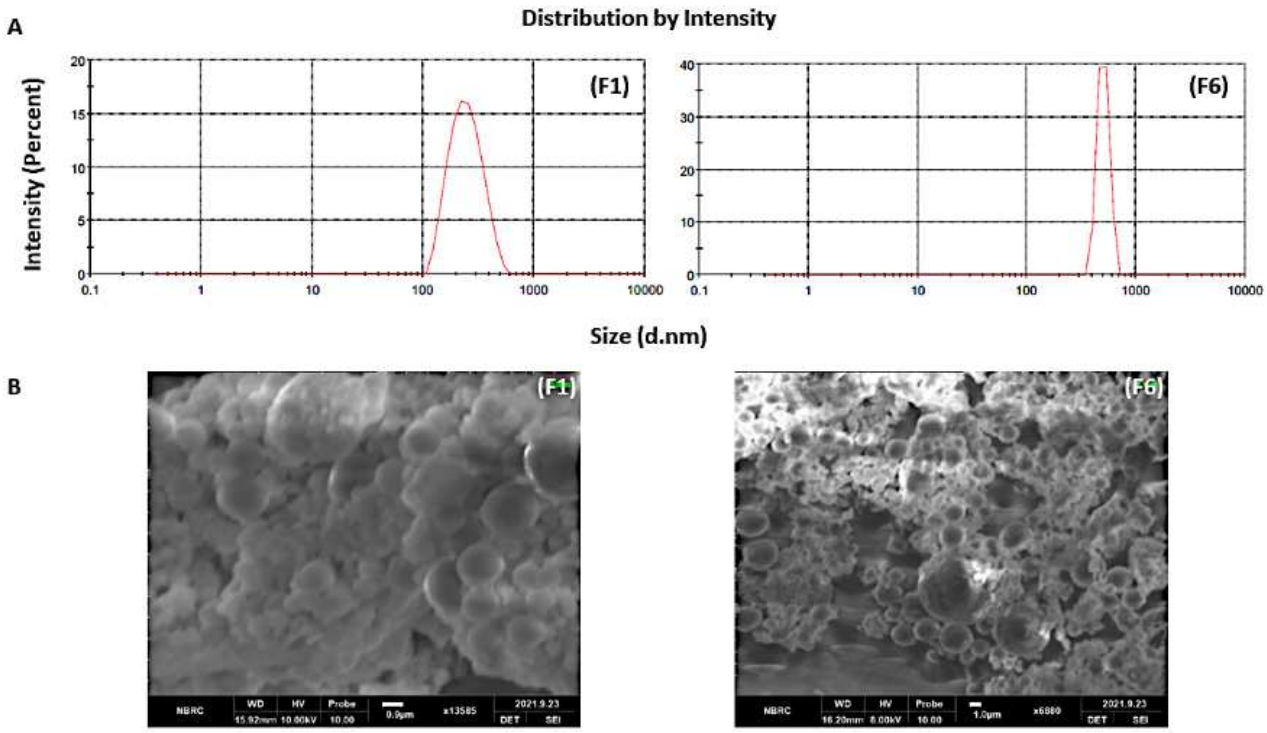

Fig. 1: Morphological assessment: (A) Hydrodynamic diameter; (B) SEM micrograph; Blank formulation (F1), Sorafenib-loaded formulation (F6).

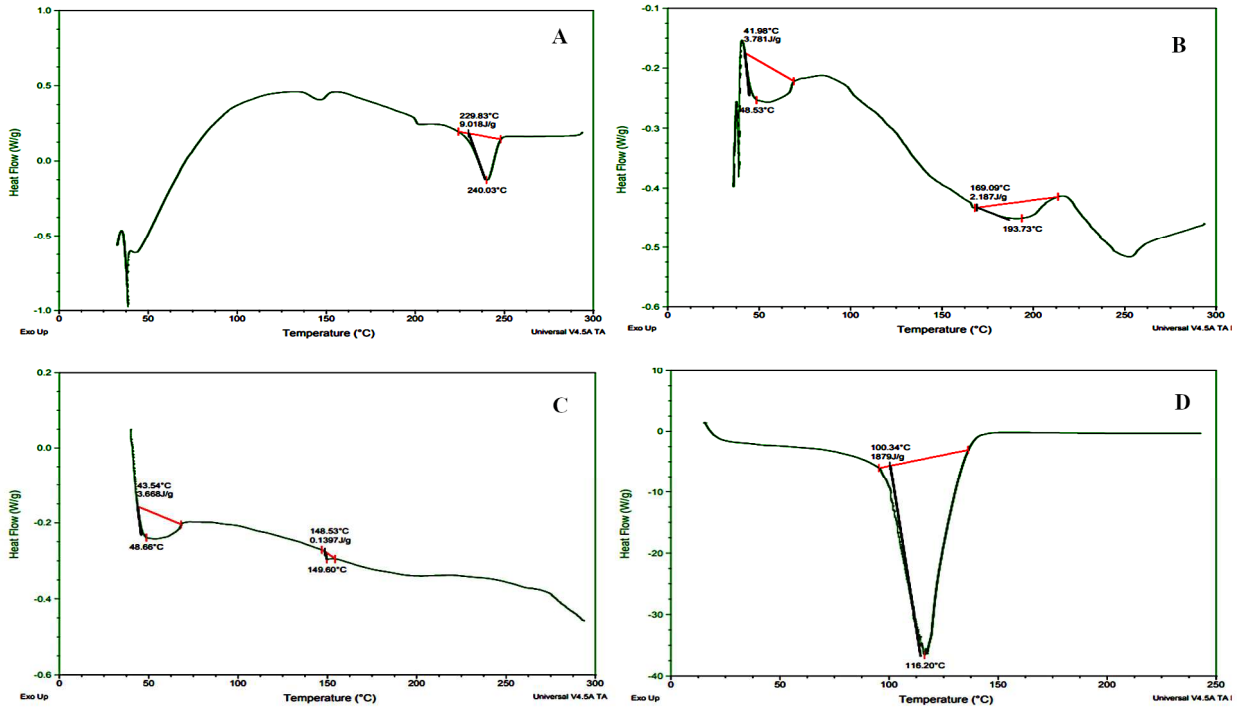

Fig. 2: DSC thermogram: (A) Sorafenib; (B) Ethyl cellulose; (C) PLGA; (D) Sorafenib-loaded formulation.

Therefore, pronounced cell shrinkage and nuclear condensation were observed in the case of F6-treated cells. SB inhibits the PI3K-Akt and RAS-RAF-MAPK downstream cellular cycles, which were accountable for cell death as a result of apoptotic body formation (Yang *et al*., 2021).

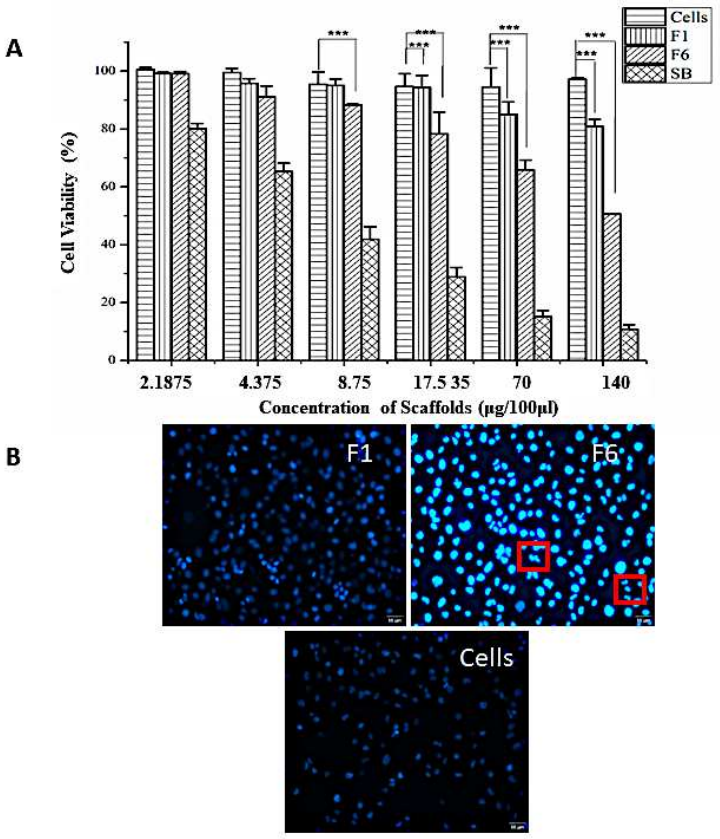

Fig. 3: Graphical representation of cell viability: (A) MTT assay; (B) Apoptotic assay. Red blocks show nuclear condensation. Blank formulation (F1), Sorafenib-loaded formulation (F6).

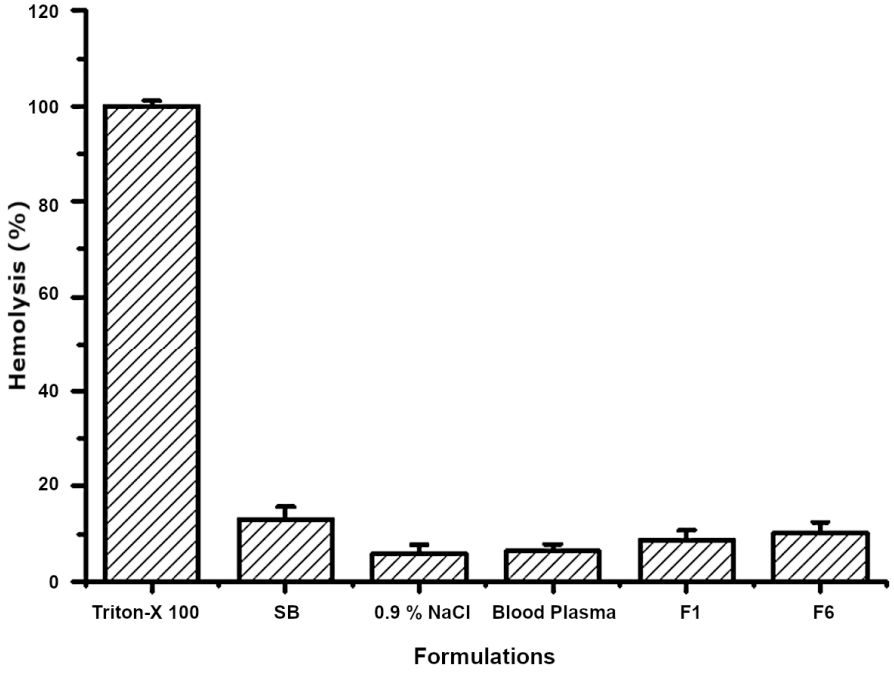

Fig. 4: Graphical representation of *ex-vivo* hemolysis assay; 1% Triton-X 100, 0.9 % NaCl, and blood plasma were used as controls for comparison with Blank formulation (F1), Sorafenib-loaded formulation (F6).

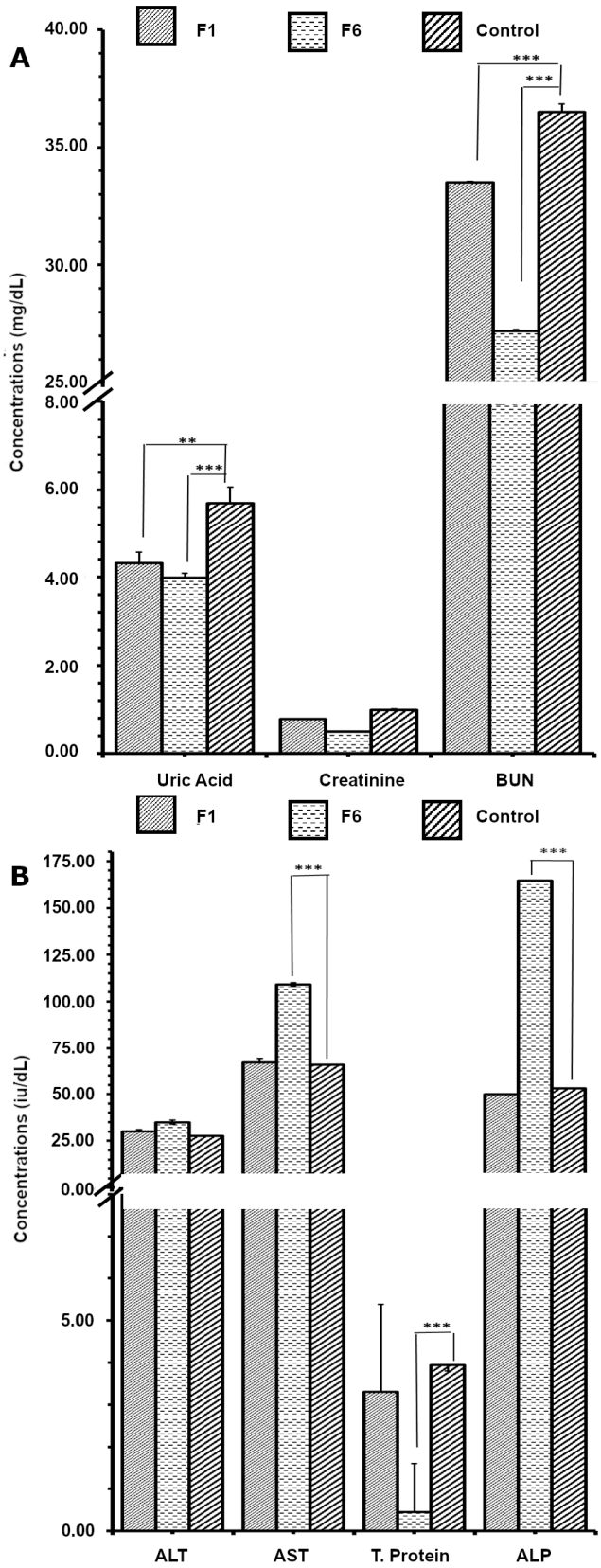

Fig. 5: Effect of formulations on clinical markers: (A) Renal function test; (B) Liver function test. Blank formulation (F1) and Sorafenib-loaded formulation (F6).

Table 2: Summary of body weight changes.

Groups	Body wt. D1* (gm ± SD)	Body wt. D7** (gm ± SD)	Change (%)
F1	32.19 ± 1.41	33.14 ± 1.89	2.87
F6	33.48 ± 4.81	32.01 ± 3.71	-4.39
Control	28.51 ± 3.67	29.78 ± 2.88	4.26

*D1: Day one of treatment; **D7: Day seven of treatment

Table 3: Summary of body viscera index after treatment.

Groups	% Weight (mean ± SD)			
	Heart	Liver	Lungs	Kidney
F1	0.56 ± 0.06	5.87 ± 0.31	0.95 ± 0.07	0.89 ± 0.07
F6	0.55 ± 0.05	5.01 ± 0.49	0.93 ±0.03	0.81 ± 0.03
Control	0.61 ± 0.01	5.42 ± 0.55	0.99 ± 0.02	0.84 ± 0.06

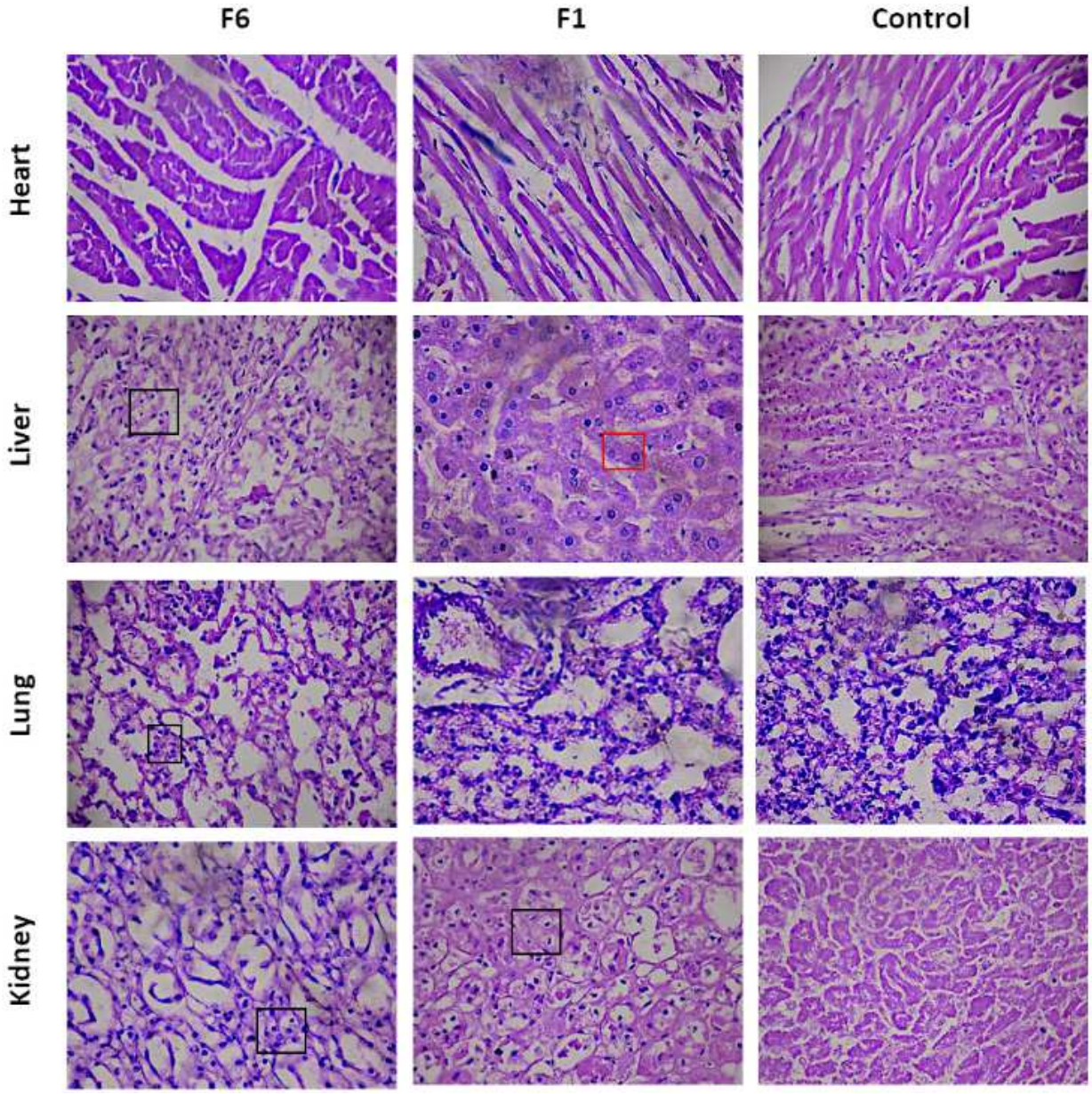

Fig. 6: Histopathological evaluation of different organs: Pyknosis (black box) and chromatin condensation (red box) are evident for Blank formulation (F1), Sorafenib-loaded formulation (F6).

Ex-vivo hemolysis assay

In a human biological system, erythrocytes are the major building blocks. They contain hemoglobin, which plays a crucial role in the transportation of oxygen and CO_2 in tissues (Chatzitaki *et al*., 2020). The hemolysis assay determines the percentage of damage to the red blood cells that bind with oxygen to make oxyhemoglobin. The absorbance of oxyhemoglobin can be interpreted spectrophotometrically at 540 nm (Blandino, Lico *et al*., 2015). For hemolysis, a positive control was used, which was 1% Triton X-100^{TM,} having the capacity to completely lyse the red blood cells. From Triton X-100^{TM}, oxyhemoglobin absorbance values were calculated and all other results were compared to these results. SB showed hemolysis of less than 20 %. Interestingly, nano-scaffolded formulations showed lower hemolytic properties, portraying 8.75 % hemolysis for F1 and 10.05 % hemolysis for F6 (Fig. 4). Therefore, these formulations can further be used for *in-vivo* evaluation.

In-vivo acute toxicity

Female BALB/c mice with an average body weight between 25 and 35 gm were treated with different formulations of nano-scaffolds and normal saline as a control with tail vein injections. These were then kept under observation for one week and no abnormal physical or behavioral change was observed. Sleep and respiration patterns were also observed for any noticeable change. A good supply of food and water was provided to minimize any malnutrition effects and all the animals were weighed before and after treatment. All these parameters remained unchanged in all cases, except for the drug-loaded nano-scaffold group. The body weight on day seven (D7) for the F6-treated group decreased by 4.39 %. On the other hand, a pronounced gain in weight was observed for the F1 and the control group, which was 2.87 % and 4.26 %, respectively (Table 2). The change in body viscera depicted the effect of formulations on the vital organs of the mice. The results showed a hallmark effect on the weight of vital organs, as shown in table 3 (Mukherje *et al*., 2021).

The assessment of the effects of the formulations was also done on the complete blood count. The result showed the presence of significant differences in control and treatment groups, with a significant level of $p < 0.001$ for WBC and hemoglobin. On the other hand, the HCT (%) level was also significant with a $p < 0.01$ (Table S2). However, all the changes were within the acceptable value range and similar results were reported in a previous study where the white blood cells and hemoglobin levels were disturbed due to the presence of SB (Hassan *et al*., 2024; Jin *et al*., 2024). The PI3k levels are also responsible for the modulation of platelets; therefore, similar results were obtained in current study and a pronounced level change was observed (Yang *et al*., 2020).

Clinical markers

Clinical markers, including renal function test and liver function test, were also evaluated to investigate the safety of formulations (Fig. 5). These included uric acid, creatinine and blood urea nitrogen (BUN) for renal function test and aspartate aminotransferase (AST), total protein, alkaline phosphatases (ALP) and alanine aminotransferase (ALT) for liver function test. A significant level of changes in F6 treated group (3.99 ± 0.10 mg/dL) was observed as compared to the control group (5.70 ± 0.357 mg/dL) in the case of uric acid ($p = 0.001$) and BUN ($p = 0.0013$) for the formulation containing the drug (F6) i.e. 27.20 ± 0.058 mg/dL as compared to control group (36.50 ± 0.351 mg/dL). These clinical levels were predictive of impaired renal function. Similar results were obtained in the case of AST and ALP ($p = 0.7099$ and 0.000, respectively) for drug-loaded formulation (66.0 ± 1.0 U/L and 164.67 ± 3.786 iu/L, respectively), where these levels increased as compared to the control group (Sun, Fang *et al*., 2021). These results represented the presence of cirrhosis and fatty liver and furthermore, these results were in good coordination with the results of the body viscera (Table 3). On the other hand, total protein content also decreased, which was an indicative factor for the diagnosis of the necrotic liver. A decrease in total serum proteins predicted the presence of liver malfunction, usually the fatty liver.

Histopathological evaluation

H and E staining was used for the histopathological evaluation of the heart, lungs, liver and kidney. A mild to moderate level of fibrosis was present in the case of SB-loaded formulations and a mild to no fibrosis was present in blank formulation-treated heart muscles (Fig. 6). Pyknosis (condensation of the nucleus), chromatin condensation, fibrosis and apoptotic bodies were observed in the case of both F1 and F6 formulations, but to a different extent. These changes were predictive of fatty liver changes and cirrhosis (Fig. 6), showing good coordination with the results of the body's visceral index and clinical markers. Some necrotic and pyknotic bodies were also obvious in the case of the drug-loaded formulation of the kidney. However, the overall changes were not to such an extent to degrade the complete tissue in any of the vital organs.

DISCUSSION

The preparation of the nano-scaffold was carried out by homogenization of phases and ultimately by phase evaporation. This resulted in the salting out of polymers and drug molecules in the presence of PVA as an emulsifier. Therefore, these factors were involved in the variation in formulation size and PDI which may be due to hydrogen-bonding regions in the structures of the formulation constituents (Phan *et al*., 2021). EE% showed the presence of 74 % of the drug molecules in the

formulation. Washing of the formulations may have parted its effect on the encapsulation of drug molecules. Some of the drug molecules present on the surfaces of the formulations were washed out during the process. DSC results also further confirmed a geometric and physical status change in the formulations in the presence of these different constituents. The peaks of formulation showed sharp endset gain, meaning in the presence of a physical mixture as amorphous as well as crystalline form. The crystalline drug molecules did not show their presence in encapsulation and were washed out (Liang *et al*., 2021; Sultan *et al*., 2022). On the other hand, it can be stated that some drug molecules were interacting with the polymeric backbone of nano-scaffolds, supporting the reasoning of a change in size and PDI of the formulation. The SEM results showed the presence of round particles as expected by the solvent evaporation method. The presence of pores on the surfaces of nano-scaffolds supported the hypothesis of the preparation of the nano-scaffolds, especially in the presence of porogen sodium chloride. A few particles were present as fused particles, which was due to the soft nature of the particles. The samples were air dried; therefore, particles settled down on stubs and under the influence of gravity, they felt stress and fused. Moreover, a range of PDIs caused the appearance of differently sized particles in micrographs. The cell culture results, besides these results, showed a viability of 50.66 ± 0.13 % in the case of drug-loaded formulation at maximum treatment concentrations, as compared to 80.91 ± 2.41 % of blank formulation at same concentration. This depicted the safety of these fabricated systems in the absence of drug, maintaining its suitability as carrier system for other therapeutic agents. Apoptotic assay, in parallel to the cell viability assay, further confirmed the presence of a condensed nucleus. DAPI stains the degraded and condensed nucleus more than the normal nucleus; hence, a more prominent dense DAPI stain was observed in the case of the drug-treated group. The possible mechanism of cell death was the formation of apoptotic bodies (condensed nucleus) along with the presence of chromatin degradation (Khan *et al*., 2021; Sarma *et al*., 2024). Before assessing the safety of the formulations, the investigations regarding the *ex vivo* hemolysis were performed, where different controls as well as formulations were used to treat RBCs. A less than 20 % hemolysis is considered to be safe. In the treatment groups, it was less than or equal to 10 % nearly every case; hence, the fabricated nano-scaffolds may be assessed further by *in-vivo* investigation. *In-vivo* results showed a decrease in the BUN levels, predicting the presence of some acute injury in the kidney or liver malfunction for drug-loaded nano-scaffolds (Hashim *et al*., 2022). These levels may further be linked with protein malnutrition or liver disorientation of the protein metabolism (Hashim *et al*., 2022; Lan *et al*., 2021; Qin *et al*., 2024). The decrease in uric acid levels is also associated with acute kidney problems or liver malfunctioning of protein metabolism (Li *et al*., 2020; Qin *et al*., 2024). On the other hand, liver function test showed an increase in levels of AST and ALP, revealing necrosis and cirrhosis. Moreover, AST/ALT levels were also higher in the case of the drug-loaded formulation group, which means a possibility of heart issues. An increase in ALP level may be indicative of liver disease; besides this, an ALT/ALP value greater than 2 was suggestive of drug-induced cholestasis. However, all these levels mean a recent acute disturbance in the liver and heart, again showing the effect of formulations (Hashim *et al*., 2022; Sharata *et al*., 2025). These results were in good coordination with the results of apoptotic assay and histopathological investigations (Fig. 6), as they reveal the presence of apoptotic bodies. Furthermore, such changes are present in the liver, heart and kidney, showing the effect of drug loaded formulation and minor changes are also present in the blank formulation. However, despite these changes, the results predicted the presence of acute toxicity that is reversible (Hassan *et al*., 2024). Therefore, the investigations can be summarized in the way that all the results were demonstrating the good entrapment of the drug, with reasonable surface morphology and safety profile of the formulations, so these formulations can be used in the future as a carrier for other drugs and for the treatment of cancer.

CONCLUSION

The main goal of the study was to encapsulate SB in nano-scaffolds. This was achieved during the current study and extensive *in-vitro* and *in-vivo* testing was performed. The presence of the drug was confirmed by encapsulation efficiency and DSC results. Furthermore, the morphological investigation by SEM showed the presence of round nano-scaffolded structures of different nanoscale sizes. The *in-vitro* cell viability and apoptotic assays showed the effects of drug molecules on viability and the nucleus. Similar results were also revealed by *in-vivo* studies, as clinical markers and histopathological investigation pointed out the presence of apoptotic bodies and the effect of formulations on different organs. Therefore, under the umbrella of these results, conclusion can be drawn that the fabrication method was successful for the drug. Furthermore, the *in-vitro* and *in-vivo* results supported the study in a way that it can be used in future studies. The application of the system for a tumor model is recommended, which can further be extended to a high set of *in-vivo* trials.

Acknowledgments
Not applicable

Authors' contributions
Arooj Khalid: Conceptualization, methodology and formal analysis; Muhammad Yasir Ali: Conceptualization, supervision, project administration, writing-review and editing; Roman tul Janat: Methodology and formal analysis; Mulazim Hussain Asim: Data curation; Ijaz Ali:

writing, data curation, critically revising manuscript; Daulat Haleem Khan: Review and editing; Umaira Rehman: Writing and review; Saima: Software and data curation; Asma Razzaq: Analysis and editing.

Funding
The work was supported by the Higher Education Commission Pakistan (20-16336/NRPU/R&D/HEC/2021 2021) and Faculty of Pharmaceutical Sciences GC University Faisalabad.

Data availability statement
All data generated or analysed during this study are included in this published article [and its supplementary information files].

Ethical approval
The animal study protocol was approved by the Ethical Committee of the Faculty of Pharmaceutical Sciences, GC University Faisalabad (AL: 00140/22/April22 and dated: 11-04-2022). This study was performed in adherence with the ARRIVE guidelines. See supplementary file for the ARRIVE checklist.

Conflicts of interest
The authors declare no conflict of interest.

Supplementary data

REFERENCES

Alawak M, Mahmoud G, Dayyih AA, Duse L, Pinnapireddy SR, Engelhardt K, Awak I, Wolk C, Konig AM and Brußler J (2020). Magnetic resonance activatable thermosensitive liposomes for controlled doxorubicin delivery. *Mater Sci and Eng, C* **115**: 111116.

Ali MY, Tariq I, Ali S, Amin MU, Engelhardt K, Pinnapireddy SR, Duse L, Schäfer J and Bakowsky U (2020). Targeted ErbB3 cancer therapy: A synergistic approach to effectively combat cancer. *Int J Pharm,* **575**: 118961.

Ali S, Amin MU, Tariq I, Sohail MF, Ali MY, Preis E, Ambreen G, Pinnapireddy SR, Jedelska J and Schafer J (2021). Lipoparticles for synergistic chemo-photodynamic therapy to ovarian carcinoma cells: *In-vitro* and *in-vivo* assessments. *Intern J Nanomed,* **16**: 951-976.

Anindyajati A, Boughton P and Ruys AJ (2022). Study on processing parameters of polycaprolactone electrospinning for fibrous scaffold using factorial design. *RETM,* **8**(2): 321-333.

Baltz N and Scherließ R (2025). Entrapment efficiency methodology for lipid nanoparticles–a literature review. *OpenNano,* **24**(2025): 100251.

Benov L (2021). Improved formazan dissolution for bacterial MTT assay. *Microbiol spectr,* **9**(3): e01637-01621.

Blandino A, Lico C, Baschieri S, Barberini L, Cirotto C, Blasi P and Santi L (2015). *In-vitro* and *in-vivo* toxicity evaluation of plant virus nanocarriers. *Colloids Surf B Biointerfaces,* **129**: 130-136.

Chatzitaki AT, Jesus S, Karavasili C, Andreadis D, Fatouros DG and Borges O (2020). Chitosan-coated PLGA nanoparticles for the nasal delivery of ropinirole hydrochloride: *In-vitro* and ex vivo evaluation of efficacy and safety. *Intern J Pharm,* **589**: 119776.

Chen Y, Han J, Wang G, Qian B and Zhao H (2022). Anticancer effects of zapotin flavone in human gastric carcinoma cells are mediated via targeting m-TOR/PI3K/AKT signalling pathway. *Acta Biochim Pol,* **69**(2): 465-469.

Donnaloja F, Jacchetti E, Soncini M and Raimondi MT (2020). Natural and synthetic polymers for bone scaffolds optimization. *Polymers,* **12**(4): 905.

Dwivedi R, Kumar S, Pandey R, Mahajan A, Nandana D, Katti DS and Mehrotra D (2020). Polycaprolactone as biomaterial for bone scaffolds: Review of literature. *J Oral Biol Craniofac Res,* **10**(1): 381-388.

Estandarte AK, Botchway S, Lynch C, Yusuf M and Robinson I (2016). The use of DAPI fluorescence lifetime imaging for investigating chromatin condensation in human chromosomes. *Sci Rep,* **6**(1): 1-12.

Gordon J and Amini S (2021). General overview of neuronal cell culture. *NSC,* **1078**: 1-8.

Guzman-Rocha DA, Cano-Gonzalez ME and Garcia-Contreras R (2025). Physicochemical properties of magnetic scaffolds with hydroxyapatite nanoparticles and chitosan. *MRS Advances,* **10**(13): 1596-1601.

Hashim M, Mujahid H, Hassan S, Bukhari S, Anjum I, Hano C, Abbasi BH and Anjum S (2022). Implication of Nanoparticles to combat chronic liver and kidney diseases: Progress and perspectives. *Biomolecules* **12**(10): 1337.

Hassan HAFM, Sedky NK, Nafie MS, Mahdy NK, Fawzy IM, Fayed TW, Preis E, Bakowsky U and Fahmy SA (2024). Sustainable nanomedicine: Enhancement of Asplatin's cytotoxicity *in-vitro* and *in-vivo* using green-synthesized zinc oxide nanoparticles formed via microwave-assisted and gambogic acid-mediated processes. *Molecules,* **29**(22): 5327.

Huang WJ, Oo TL, He HY, Wang AQ, Zhan J, Li CZ, Wei SQ and He LF (2014). Aluminum induces rapidly mitochondria-dependent programmed cell death in Al-sensitive peanut root tips. *Bot Stud,* **55**(1): 1-12.

Jamil A, MN P, Lee DW, Li M, Yu R and Song JI (2026). Improvement of mode-II fracture toughness of carbon fiber and carbon/flax fiber hybrid composites using cellulose nanofibers. *Mech Adv Mater Struct,* **33**(1): 2615050.

Jin K, Liao YC, Cheng TC, Li X, Lee WJ, Pi F, Jasinski D, Chen LC, Phelps MA, Ho YS and Guo P (2024). *In-vitro* and *in-vivo* evaluation of the pathology and safety aspects of three- and four-way junction RNA nanoparticles. *Mol Pharm,* **21**(2): 718-728.

Khan MJ, Ahmad A, Khan MA and Siddiqui S (2021). Zinc oxide nanoparticle induces apoptosis in human epidermoid carcinoma cells through reactive oxygen species and DNA degradation. *Biol Trace Elem Res,* **199**(6): 2172-2181.

Kus-Liśkiewicz M, Fickers P and Ben Tahar I (2021). Biocompatibility and cytotoxicity of gold nanoparticles: Recent advances in methodologies and regulations. *Intern J Mol Sci,* **22**(20): 10952.

Lan Q, Zheng L, Zhou X, Wu H, Buys N, Liu Z, Sun J and Fan H (2021). The value of blood urea nitrogen in the prediction of risks of cardiovascular disease in an older population. *Front Cardiovasc Med,* **8**: 614117.

Li M, Ye ZC, Li CM, Zhao WB, Tang H, Liu X, Peng H and Lou TQ (2020). Low serum uric acid levels increase the risk of all-cause death and cardiovascular death in hemodialysis patients. *Renal failure,* **42**(1): 315-322.

Li Y, Liu W, Wang Y and Lu S (2025). Cellulose based nano-scaffolds for targeted cancer therapies: Current status and future perspective. *Intern J Nanomed,* **20**: 199-213.

Liang SX, Zhang LC, Reichenberger S and Barcikowski S (2021). Design and perspective of amorphous metal nanoparticles from laser synthesis and processing.*PCCP,* **23**(19): 11121-11154.

Lu Y, Zhang R, Jia Y, Gao Y and Mao L (2023). Effects of nanoparticle types and internal phase content on the properties of W/O emulsions based on dual stabilization mechanism. *Food Hydrocoll,* **139**: 108563.

Malik MK, Bhatt P, Singh J, Kaushik RD, Sharma G and Kumar V (2022). Preclinical safety assessment of chemically cross-linked modified mandua starch: Acute and sub-acute oral toxicity studies in Swiss albino mice. *ACS Omega,* **7**(40): 35506-35514.

Mohaghegh S, Nokhbatolfoghahaei H, Baniameri S, Farajpour H, Fakhr MJ, Shokrolahi F and Khojasteh A (2024). Physicochemical and biological characterization of gelatin/alginate scaffolds reinforced with β-TCP, FDBA, and SRHA: Insights into stem cell behavior and osteogenic differentiation. *Intern J Biomat,* **2024**(1): 1365080.

Mukherjee S, Bollu VS, Roy A, Nethi SK, Madhusudana K, Kumar JM, Sistla R and Patra CR (2021). Acute toxicity, biodistribution, and pharmacokinetics studies of pegylated platinum nanoparticles in mouse model. *Adv Nanobiomed Res,* **1**(7): 2000082.

Phan C, Shen J, Yu K, Liu J and Tang G (2021). Hydrogen bonds, topologies, energy frameworks and solubilities of five Sorafenib salts. *Intern J Mol Sci,* **22**(13): 6682.

Qin W, Huang J, Zhang M, Xu M, He J and Liu Q (2024). Nanotechnology-based drug delivery systems for treating acute kidney injury. *ACS Biomat Sci and Eng,* **10**(10): 6078-6096.

Sarma S, Thakur N, Varshney N, Jha HC and Sarma TK (2024). Chromatin inspired bio-condensation between biomass DNA and guanosine monophosphate produces all-nucleic hydrogel as a hydrotropic drug carrier. *Commun Chem,* **7**(1): 261.

Sathish T, Ramsamy M, Manikandan ideationIP PR and Raja S (2022). Nano, micro, and macro materials in scaffolds for biomedical applications: A review. *Biomed J Sci Tech Res,* **46**: 37455-37470.

Sharata EE, Attya ME, Khalaf MM, Rofaeil RR, Hemeida RA and Abo-Youssef AM (2025). Unraveling chemotherapy-evoked hepatic dysfunction: A deep dive into cyclophosphamide-related liver injury. *Naunyn-Schmiedeberg's Arch. Pharmacol,* **399**: 1-16.

Sultan MH, Moni SS, Madkhali OA, Bakkari MA, Alshahrani S, Alqahtani SS, Alhakamy NA, Mohan S, Ghazwani M, Bukhary HA, Almoshari Y, Salawi A and Alshamrani M (2022). Characterization of cisplatin-loaded chitosan nanoparticles and rituximab-linked surfaces as target-specific injectable nano-formulations for combating cancer. *Sci Rep,* **12**(1): 468.

Sun R, Fang L, Lv X, Fang J, Wang Y, Chen D, Wang L, Chen J, Qi Y, Tang Z, Zhang J and Tian Y (2021). *In-vitro* and *in-vivo* evaluation of self-assembled chitosan nanoparticles selectively overcoming hepatocellular carcinoma via asialoglycoprotein receptor. *Drug Deliv,* **28**(1): 2071-2084.

Tong J, Jang SR and Park CH (2025). Zein-modified ethyl cellulose scaffolds with controlled doxycycline release and biocompatibility via a portable electrospinning device. *Mate Let,* **405**: 139659.

Tupe A, Patole V, Ingavle G, Kavitkar G, Mishra Tiwari R, Kapare H, Baheti R and Jadhav P (2024). Recent advances in biomaterial-based scaffolds for guided bone tissue engineering: Challenges and future directions. *Polym Adv Technol,* **35**(11): e6619.

Wu K-W, Sweeney C, Dudhipala N, Lakhani P, Chaurasiya ND, Tekwani BL and Majumdar S (2021). Primaquine loaded solid lipid nanoparticles (SLN), nanostructured lipid carriers (NLC), and nanoemulsion (NE): effect of lipid matrix and surfactant on drug entrapment, *In-vitro* release, and ex vivo hemolysis. *AAPS PharmSciTech,* **22**(7): 1-12.

Yang M, Liu Q, Niu T, Kuang J, Zhang X, Jiang L, Li S, He X, Wang L and Li J (2020). Trp53 regulates platelets in bone marrow via the PI3K pathway. *Exp Ther Med,* **20**(2): 1253-1260.

Yang Q, Gao L, Huang X, Weng J, Chen Y, Lin S and Yin Q (2021). Sorafenib prevents the proliferation and induces the apoptosis of liver cancer cells by regulating autophagy and hypoxia-inducible factor-1. *Exp Ther Med,* **22**(3): 980.

Yu J, Wang L, Xie X, Zhu W, Lei Z, Lv L, Yu H, Xu J and Ren J (2023). Multifunctional nanoparticles codelivering doxorubicin and amorphous calcium

carbonate preloaded with indocyanine green for enhanced chemo-photothermal cancer therapy. *Int J Nanomed,* **18**: 323-337.

Zengin Kurt B, Ozturk Civelek D, Cakmak EB, Kolcuoglu Y, Senol H, Saglık Ozkan BmN, Dag A and Benkli K (2024). Synthesis of sorafenib− ruthenium complexes, investigation of biological activities and applications in drug delivery systems as an anticancer agent. *J M,ed Chemy,* **67**(6): 4463-4482.

Zhu P, Zhang H and Lu H (2021). Preparation of polyetherimide nanoparticles by a droplet evaporation-assisted thermally induced phase-separation method. *Polymers,* **13**(10): 1548.